

University of Groningen

## Anisotropic Hanle line shape via magnetothermoelectric phenomena

Das, Kumar; Dejene, Fasil; van Wees, Bart; Vera Marun, Ivan

*Published in:*  
Physical Review. B: Condensed Matter and Materials Physics

*DOI:*  
[10.1103/PhysRevB.94.180403](https://doi.org/10.1103/PhysRevB.94.180403)

**IMPORTANT NOTE:** You are advised to consult the publisher's version (publisher's PDF) if you wish to cite from it. Please check the document version below.

*Document Version*  
Final author's version (accepted by publisher, after peer review)

*Publication date:*  
2016

[Link to publication in University of Groningen/UMCG research database](#)

*Citation for published version (APA):*

Das, K., Dejene, F., van Wees, B., & Vera Marun, I. (2016). Anisotropic Hanle line shape via magnetothermoelectric phenomena. *Physical Review. B: Condensed Matter and Materials Physics*, 94. <https://doi.org/10.1103/PhysRevB.94.180403>

**Copyright**

Other than for strictly personal use, it is not permitted to download or to forward/distribute the text or part of it without the consent of the author(s) and/or copyright holder(s), unless the work is under an open content license (like Creative Commons).

The publication may also be distributed here under the terms of Article 25fa of the Dutch Copyright Act, indicated by the "Taverne" license. More information can be found on the University of Groningen website: <https://www.rug.nl/library/open-access/self-archiving-pure/taverne-amendment>.

**Take-down policy**

If you believe that this document breaches copyright please contact us providing details, and we will remove access to the work immediately and investigate your claim.

*Downloaded from the University of Groningen/UMCG research database (Pure): <http://www.rug.nl/research/portal>. For technical reasons the number of authors shown on this cover page is limited to 10 maximum.*

# Anisotropic Hanle line shape via magnetothermoelectric phenomena

K. S. Das,<sup>1,\*</sup> F. K. Dejene,<sup>2</sup> B. J. van Wees,<sup>1</sup> and I. J. Vera-Marun<sup>1,3,†</sup>

<sup>1</sup>*Zernike Institute for Advanced Materials, University of Groningen, 9747 AG Groningen, The Netherlands*

<sup>2</sup>*Max Planck Institute of Microstructure Physics, D-06120 Halle, Germany*

<sup>3</sup>*School of Physics and Astronomy, University of Manchester, Manchester M13 9PL, UK*

We observe anisotropic Hanle lineshape with unequal in-plane and out-of-plane non-local signals for spin precession measurements carried out on lateral metallic spin valves with transparent interfaces. The conventional interpretation for this anisotropy corresponds to unequal spin relaxation times for in-plane and out-of-plane spin orientations as for the case of 2D materials like graphene, but it is unexpected in a polycrystalline metallic channel. Systematic measurements as a function of temperature and channel length, combined with both analytical and numerical thermoelectric transport models, demonstrate that the anisotropy in the Hanle lineshape is magneto-thermal in origin, caused by the anisotropic modulation of the Peltier and Seebeck coefficients of the ferromagnetic electrodes. Our results call for the consideration of such magnetothermoelectric effects in the study of anisotropic spin relaxation.

Electrical spin injection and detection in non-local lateral spin valves have been used extensively to study pure spin currents in non-magnetic (NM) materials [1–8]. Hanle measurements allow the manipulation of the spin accumulation in the NM materials via a perpendicular magnetic field, which induces spin precession as the carriers diffuse along the NM channel. From these experiments, we can extract the spin transport parameters of the channel, like the spin relaxation length and time, and hence get an insight about the nature of spin-orbit interaction (SOI) causing spin relaxation. This is particularly relevant for 2D materials like graphene, where the SOI acting along the in-plane and out-of-the plane directions can differ and lead to anisotropic spin relaxation, manifested by different signals for the in-plane and out-of-plane spin configurations in the Hanle experiments [9, 10]. In contrast, for polycrystalline films, spin relaxation is expected to be isotropic [11].

In this work we use metallic non-local spin valves (NLSVs), with aluminium (Al) as the NM material, to study spin precession as a function of temperature. Permalloy ( $\text{Ni}_{80}\text{Fe}_{20}$ , Py) has been used as the ferromagnetic (FM) electrodes to inject a spin-polarized current into Al across a transparent interface and to non-locally detect the non-equilibrium spin accumulation in Al at a distance  $L$  from the injector. This model system with transparent FM/NM interfaces has been thoroughly studied via spin valve measurements. But curiously, corresponding spin precession studies in such systems are scarce. Only recently a few groups have demonstrated spin precession in NLSVs with transparent FM/NM interfaces [12, 13], with the NM channel being either silver or copper. More importantly, these few experiments have been done only at low temperatures ( $T \leq 10$  K), with no reports on Hanle measurements at room temperature for transparent FM/NM interfaces.

We demonstrate, through non-local spin precession experiments on Py/Al NLSVs with transparent interfaces, an anomalous Hanle lineshape for  $T > 150$  K,

in which the in-plane and out-of-plane spin signals are unequal. This anisotropic Hanle lineshape generally indicates different spin relaxation rates for spins aligned parallel and perpendicular to the plane of the NM channel [9, 10]. However, anisotropic spin relaxation in a polycrystalline metallic film has not been observed in the literature and is unexpected, especially being stronger at higher temperatures. Such a temperature dependence of the anisotropy is indicative of a thermoelectric origin. With the help of analytical and numerical thermoelectric transport models, we ascribe the anisotropy in the Hanle measurements to a change in the baseline resistance [14] due to the anisotropy in the Seebeck and Peltier coefficients of the FM. The results evidence how an apparent anisotropic spin precession can develop in an isotropic NM channel, via the coexistence of spin and heat currents and spin-orbit coupling in the FM.

Py/Al NLSVs with transparent interfaces (interface resistance  $< 10^{-15} \Omega \cdot \text{m}^2$ ) and varying injector-detector separations ( $L$ ) were prepared on top of a 300 nm thick  $\text{SiO}_2$  layer on a Si substrate. The device preparation is described in detail in the supplementary material [15] and follows Refs. [6, 13, 14]. Fig. 1(a) shows an SEM image of a representative NLSV along with the electrical connections for spin-valve and Hanle measurements. A low frequency (13 Hz) alternating current ( $I = 400 \mu\text{A}$ ) was applied between the injector (Py1) and the left end of the Al channel. The first harmonic response of the corresponding non-local signal ( $R_{\text{NL}} = V_{\text{NL}}/I$ ) was measured between the detector (Py2) and the right end of the Al channel by standard lock-in technique.

The NLSVs were first characterized via spin-valve measurements as shown in Fig. 1(b). An external magnetic field ( $B_y$ ) was swept along the main axis of the FMs to orient their magnetization in either parallel (P) or anti-parallel (AP) configurations, corresponding to distinct levels  $R_{\text{NL}}^{\text{P}}$  and  $R_{\text{NL}}^{\text{AP}}$  in the non-local response. From these measurements we extracted the spin accumulation signal in the Al channel,  $R_{\text{S}} = R_{\text{NL}}^{\text{P}} - R_{\text{NL}}^{\text{AP}}$ , and the base-

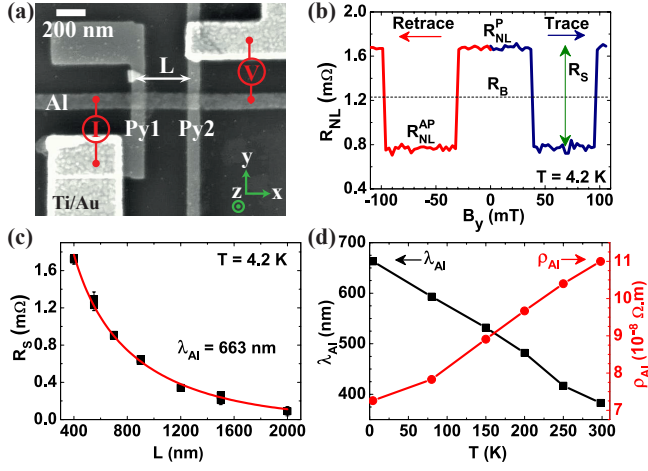


FIG. 1. (a) An SEM image of a representative NLSV along with the electrical connections for spin-valve and Hanle measurements. Py1 and Py2 act as spin injector and detector, respectively, separated by a distance  $L$ . (b) Spin-valve measurement on a device with  $L = 700$  nm at  $T = 4.2$  K. The parallel ( $R_{NL}^P$ ) and anti-parallel ( $R_{NL}^{AP}$ ) states are shown along with the baseline resistance ( $R_B$ ) and the spin accumulation signal ( $R_S$ ). (c) Dependence of  $R_S$  on  $L$ , used to extract the spin relaxation length in Al ( $\lambda_{Al}$ ), by fitting the data (black squares) with a spin diffusion model (red line) as described in the text. The error bars correspond to the noise (standard deviation) in the spin-valve curves when quantifying  $R_{NL}^P$  and  $R_{NL}^{AP}$  signals. (d) Temperature dependence of  $\lambda_{Al}$  and the resistivity of the Al channel ( $\rho_{Al}$ ).

line resistance,  $R_B = (R_{NL}^P + R_{NL}^{AP})/2$  (which later will be used to interpret the spin precession measurements). The spin accumulation created at the injector junction decays exponentially in the Al channel with a characteristic spin relaxation length,  $\lambda_{Al}$ . Fig. 1(c) shows the dependence of  $R_S$  on the injector-detector separation ( $L$ ), from which  $\lambda_{Al}$  can be extracted using the standard spin diffusion formalism for transparent contacts [16–18]. We extracted  $\lambda_{Al}$  to be 663 nm at 4.2 K and 383 nm at 300 K. A systematic study of the temperature dependence of  $\lambda_{Al}$  revealed its monotonic decrease with increasing  $T$ , with an opposite behaviour for the resistivity of the channel ( $\rho_{Al}$ ), as shown in Fig. 1(d). These results are consistent with Elliott-Yafet spin relaxation mechanism dominated by electron-phonon interaction in bulk metal [8, 11, 19], in which the spin relaxation length is proportional to the electron mean free path.

Next, we perform Hanle spin precession measurements, in which a perpendicular magnetic field ( $B_z$ ) induces the spins injected into the Al channel to precess at a Larmor frequency  $\omega_L = g\mu_B B_z/\hbar$ , where  $g \approx 2$  is the  $g$ -factor in Al,  $\mu_B$  is the Bohr magneton and  $\hbar$  is the reduced Planck constant. As shown in Fig. 2(a-d), Hanle measurements can be performed with the magnetizations of the FMs initially aligned in-plane (at  $B_z = 0$ ) and set either parallel (P) or anti-parallel (AP) with respect to each other. The

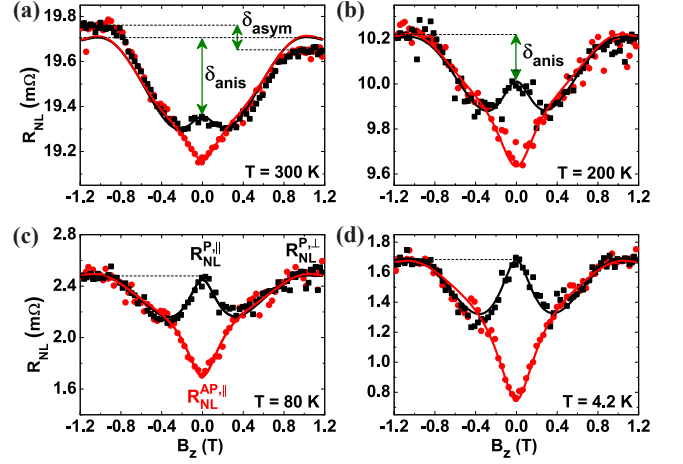


FIG. 2. Hanle measurements in a NLSV with  $L = 700$  nm at different temperatures: (a)  $T = 300$  K, (b)  $T = 200$  K, (c)  $T = 80$  K and (d)  $T = 4.2$  K. The initial magnetic configuration of the FM contacts at  $B_z = 0$  is in-plane and either parallel ( $R_{NL}^P$ , black squares) or anti-parallel ( $R_{NL}^{AP}$ , red circles), whereas for  $|B_z| > 0.9$  T it is out-of-plane and parallel ( $R_{NL}^{P,\parallel}$ ) or anti-parallel ( $R_{NL}^{AP,\parallel}$ ). The anisotropy ( $\delta_{anis}$ ) in the non-local signal ( $R_{NL}$ ) between spins oriented in-plane (y) and out-of-plane (z) is observed at 300 K and 200 K, but it is absent at 80 K and 4.2 K. The solid lines are fits to the Hanle data (see text).

Larmor precession and the resulting spin dephasing, lead to a decrease (increase) in the signal  $R_{NL}$  with increasing  $|B_z|$  for the P (AP) configuration, eventually intersecting the AP (P) curve for an average spin rotation of  $\pi/2$ . After the intersection of the P and AP curves, they bend upwards with increasing  $|B_z|$  and finally saturate for  $|B_z| \geq 0.9$  T. This happens because the magnetization of Py starts to rotate out-of-plane and finally aligns with  $B_z$  for  $|B_z| \geq 0.9$  T. The rotation of Py's magnetization with  $B_z$  can be checked from the anisotropic magnetoresistance (AMR) measurements of the Py wire, described in the supplementary material [15] and follows Refs. [3, 20]. Thus, for  $|B_z| \geq 0.9$  T, the spins are injected (and detected) in the out-of-plane (z) direction and there should be no precession caused by  $B_z$ . For isotropic spin relaxation and parallel orientation of the magnetizations, the signal  $R_{NL}^{P,\parallel}$  for spins injected in-plane at  $B_z = 0$  should be equal to the signal  $R_{NL}^{P,\perp}$  when spins are injected out-of-plane at  $|B_z| \geq 0.9$  T. We indeed observe that  $R_{NL}^{P,\parallel} = R_{NL}^{P,\perp}$  for the Hanle data at 80 K and 4.2 K (Fig. 2(c) and (d)). These Hanle data were fitted with an analytical expression obtained by solving the Bloch equation considering spin precession, diffusion and relaxation for transparent contacts [13, 21] and taking into account the out-of-plane rotation of the Py magnetization [3]. From the fitting, we obtained  $\lambda_{Al}$  to be 688 nm at 4.2 K and 544 nm at 80 K, which are comparable to the values obtained from the spin-valve measurements (Fig. 1(d)).

At higher temperatures ( $T \geq 150$  K), we notice a significant difference between  $R_{\text{NL}}^{\text{P},\parallel}$  and  $R_{\text{NL}}^{\text{P},\perp}$ , leading to anisotropic Hanle lineshapes as shown in Figs. 2(a) and (b). Such Hanle lineshapes have been hitherto associated with anisotropic spin relaxation [9, 10], in which the NM channel has different spin relaxation times for the in-plane and out-of-plane spin directions. For isotropic and polycrystalline metallic films, as is the case for our 50 nm thick Al channel, the transverse and longitudinal spin relaxation times are expected to be equal [11]. Moreover, by increasing the temperature we expect any anisotropy to decrease due to the thermal disorder in the system. Hence we rule out anisotropic spin relaxation in our system and investigate other causes for the observed Hanle lineshapes. Further checks were performed to rule out: (i) the role of interfacial roughness and magnetic impurities by probing the presence of inverted Hanle response [22, 23] in the spin-valve measurements at high in-plane fields ( $B_y$ ), (ii) non-linear effects by measuring higher harmonics and at different current densities, (iii) current inhomogeneity at the contacts and (iv) frequency dependence. For details of these further checks, see the supplementary material [15].

We quantify the anisotropy in the Hanle measurements by the parameter  $\delta_{\text{anis}} = R_{\text{NL}}^{\text{P},\perp} - R_{\text{NL}}^{\text{P},\parallel}$ , as shown in Figs. 2(a) and (b). We note that concurrent to this anisotropy we also observe a smaller asymmetry with the sign of  $B_z$ ,  $\delta_{\text{asym}} = R_{\text{NL}}^{\text{P},\perp}(B_z < -0.9 \text{ T}) - R_{\text{NL}}^{\text{P},\perp}(B_z > 0.9 \text{ T})$ , as shown in Fig. 2(a). Since  $\delta_{\text{asym}} \ll \delta_{\text{anis}}$  we focus the discussion below on the anisotropy ( $\delta_{\text{anis}}$ ).

A marked non-linear increase with temperature is observed on both the anisotropy  $\delta_{\text{anis}}$  (extracted from Hanle measurements), and the baseline resistance  $R_B$  (obtained from spin-valve measurements) in the measurements summarized in Fig. 3(a-b). We interpret these observations as an indication for a common thermal origin for both effects. Note that these trends are inconsistent with an effect purely related to spin currents, as  $\lambda_{\text{Al}}$  decreases at higher  $T$  (Fig. 1(d)). Furthermore, the trends are also inconsistent with the trivial effect of AMR on local charge currents, because the AMR has also an opposite trend with temperature (Fig. 3(c)). We remark that the origin of  $R_B$  in NLSVs has been identified as thermoelectric in nature [14]. It is driven by the interplay of Peltier cooling and heating at the injector junction, in which a charge current across the junction results in a temperature difference, and the Seebeck effect at the detector junction, which acts as a nanoscale thermocouple to electrically detect the non-local heat currents. Here, we hypothesize that the anisotropy  $\delta_{\text{anis}}$  is also thermoelectric in nature, in particular given the striking observation of an almost constant ratio  $\delta_{\text{anis}}/R_B \approx 2\%$  independent of  $L$  and  $T$ , as shown in Fig. 3(d).

To further understand the origin of the anisotropy  $\delta_{\text{anis}}$ , we must note that  $|B_z|$  modulates the magnetiza-

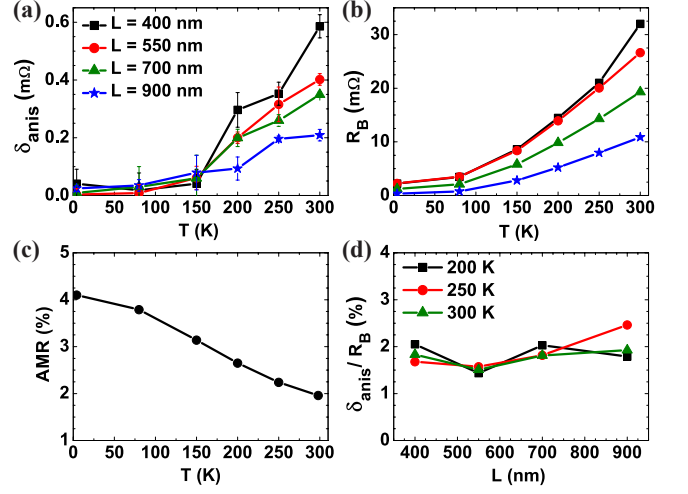


FIG. 3. Temperature ( $T$ ) dependence of: (a) The anisotropy ( $\delta_{\text{anis}}$ ) extracted from Hanle measurements for different channel lengths ( $L$ ), (b) The baseline resistance ( $R_B$ ) extracted from spin-valve measurements, and (c) Anisotropic magnetoresistance (AMR) of Py. (d) A constant ratio  $\delta_{\text{anis}}/R_B \approx 2\%$  is observed, independent of  $L$  and  $T$ .

tion direction of Py, which together with Al forms thermoelectric junctions. Similarly as the electrical resistance of Py gets modulated due to AMR, we consider here a modulation in the Seebeck ( $S$ ) and Peltier ( $\Pi$ ) coefficients as a function of the angle between the magnetization and the heat current, i.e. anisotropic thermoelectric transport due to spin-orbit interaction in the FM [24–27]. To test this hypothesis, we develop a thermoelectric model to estimate  $R_B$  in our NLSVs, and relate its corresponding magnetothermoelectric effect to  $\delta_{\text{anis}}$ .

The Peltier effect at the injector junction results in a temperature difference ( $\Delta T$ ), with respect to the reference temperature ( $T$ ), equal to

$$\Delta T = \dot{Q} R_{\text{th}} = (\Pi_{\text{Al}} - \Pi_{\text{Py}}) I R_{\text{th}}, \quad (1)$$

where  $\dot{Q}$  is the rate of Peltier heating for a current ( $I$ ) from Al into Py,  $\Pi_{\text{Al(Py)}}$  is the Peltier coefficient of Al (Py), and  $R_{\text{th}}$  is the total thermal resistance at the Py/Al junction. In analogy to the standard spin diffusion formalism used to calculate spin resistance  $R_S$  [16, 28], we implement an analytical heat diffusion model that allows us to calculate  $R_{\text{th}}$  [15, 29]. Common to both models, such a resistance is dependent on the corresponding conductivity and the characteristic decay length of the corresponding accumulation. For the thermal model, we consider the thermal conductivity  $\kappa$  and a thermal transfer length  $L_T$  given by the non-conserved heat current along the metal channel due to the heat flow into the  $\text{SiO}_2/\text{Si}$  substrate [15, 29, 30], which leads to  $L_T \approx 900$  nm in the Al channel at 300 K. The total thermal resistance experienced at the injector junction is  $R_{\text{th}} \approx 8.8 \times 10^5 \text{ K/W}$ , which is dominated by the higher  $\kappa$  of the Al channel.



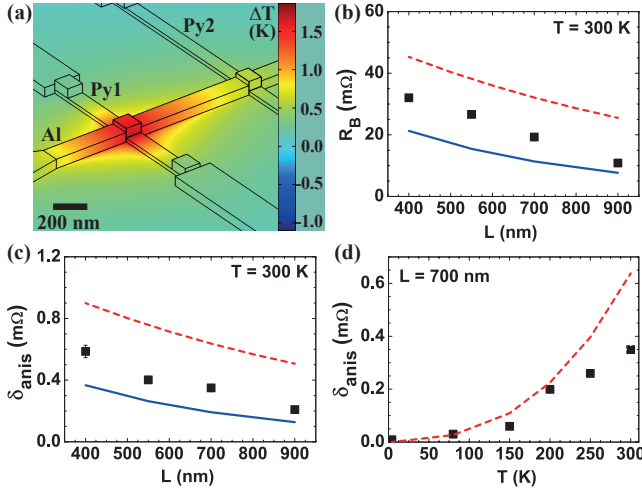


FIG. 4. (a) The temperature difference ( $\Delta T$ ) in the device area, simulated by 3-dimensional finite element modelling (3D-FEM), is shown as a colour map. Comparison between the measured data (black squares), the analytical model (red dashed lines) and 3D-FEM (blue solid lines) is presented for the dependence of the: (b) Baseline resistance ( $R_B$ ) and (c) Anisotropy ( $\delta_{\text{anis}}$ ) on the channel length ( $L$ ) at 300 K. (d) Temperature dependence of  $\delta_{\text{anis}}$ , obtained experimentally and through the analytical model, for a fixed channel length of 700 nm.

From Eq. 1, the temperature difference at the injector was found to be  $\Delta T \approx 1.7$  K, which is in good agreement with the temperature profile of the device area as shown in Fig. 4(a) (simulated by 3-dimensional finite element modelling, described later in the text). A non-local Seebeck signal  $V_{\text{th}}$  is generated due to  $\Delta T$  at a distance  $L$  from the injector, given by

$$V_{\text{th}} = (S_{\text{Al}} - S_{\text{Py}})\Delta T e^{-L/L_T}. \quad (2)$$

The modelled thermal signal ( $V_{\text{th}}/I$ ) is shown as a function of  $L$  in Fig. 4(b), together with the experimental baseline resistance ( $R_B$ ). The agreement confirms the thermoelectric origin of the latter, with  $R_B \approx V_{\text{th}}/I$ . The measured first harmonic response shown in Figs. 3 and 4 is in the linear regime accounting only for the Peltier heating/cooling and therefore excludes Joule heating. Without having used any fitting parameters, our analytical model is accurate within a factor of 2 of the experimentally obtained results. This model disregards lateral heat spreading in the narrow channel and hence serves as an upper estimate of  $R_B$  [15, 29, 30]. Furthermore, considering the Thomson-Onsager relation  $\Pi = ST$  and a linear temperature dependence of the Seebeck coefficient, we predict a non-linear dependence of  $R_B$ , which is also substantiated by the measurements in Fig. 3(b).

We address next our central hypothesis that the anisotropy in the Hanle measurements ( $\delta_{\text{anis}}$ ) emerges via the anisotropy in the thermoelectric coefficients of Py. To account for these magnetothermoelectric effects

[24, 26], we relate the isotropic ( $R_B$ ) and the anisotropic ( $\delta_{\text{anis}}$ ) thermoelectric signals, since from Eqs. 1 and 2 and the Thomson-Onsager relation, we find that  $V_{\text{th}} \propto \Pi_{\text{Py}} \cdot S_{\text{Py}} \propto \Pi_{\text{Py}}^2$ . This allows us to explain the ratio  $\delta_{\text{anis}}/R_B \approx 2\%$ , observed in Fig. 3d, by considering an anisotropy in the thermoelectric coefficients of Py ( $\Pi_{\text{Py}}$ ,  $S_{\text{Py}}$ ) of approximately 1%. This direct extraction of the anisotropy,  $\Delta\Pi_{\text{Py}}/\Pi_{\text{Py}} \approx 1\%$ , allows us to successfully model both the channel length ( $L$ ) and temperature ( $T$ ) dependence of the thermoelectric signals, as shown in Fig. 4(b-d). Our observation of 1% anisotropic magnetothermopower in Py is in agreement with previous studies on Ni nanowires which put a limit of upto 10% [24, 26].

For completeness, we consider a different anisotropic effect: the modulation in the thermal conductivity of Py, and hence on  $R_{\text{th}}$ , as a consequence of AMR and the Wiedemann-Franz law. Taking the measured AMR = 2% at room temperature as an upper limit [27], we obtain an anisotropy which is lower by an order of magnitude than the measured one, and therefore cannot account for the observations. The negligible modulation via this effect is understood by the dominant role of the Al channel (which has no AMR) in determining the total  $R_{\text{th}}$ .

Finally, an accurate 3-dimensional finite element model (3D-FEM) was developed incorporating the physics of both the anisotropy of the thermoelectric coefficients and of AMR. It is seen in Fig. 4(b)-(c) that the 3D-FEM shows a good agreement with the data. A detailed description of the model is included in the supplementary material [15]. Having established the thermal origin of the baseline resistance and the anisotropy, we use this 3D-FEM to explore the asymmetry ( $\delta_{\text{asym}}$ ) observed in the Hanle measurement at 300 K. A finite component of the heat current in the Py bar at the detector junction flowing along the length of the Al channel, combined with the Py magnetization pointing in the out-of-plane direction, generates a transversal voltage along the main axis of the Py bar due to the anomalous Nernst effect [25, 31]. This transversal voltage gives rise to the asymmetry observed in the Hanle measurements. We successfully account for  $\delta_{\text{asym}}$  by considering an anomalous Nernst coefficient of Py equal to 0.06, a factor of two smaller than obtained earlier in Py/Cu spin valves [25].

The magnetothermoelectric effects here described are general phenomena in Hanle experiments. Note that the use of tunnel interfaces in previous studies [3, 9, 10] enhances the spin signal by about 100 times, but from our thermal model that would only amount to an enhancement of the thermoelectric response by a factor of 1. This allows us to understand why the anisotropic signatures have not been identified in previous studies, as the thermoelectric response would only be a modulation of approximately 1% relative to the spin dependent Hanle signal in those studies. In this work, with transparent contacts and at room temperature, the spin signals are comparable to the thermoelectric effects, making the latter

relevant for correct interpretation of the spin-dependent signals.

We thank J. G. Holstein, H. M. de Roos, H. Adema and T. Schouten for their technical assistance. We acknowledge the financial support of the Zernike Institute for Advanced Materials and the Future and Emerging Technologies (FET) programme within the Seventh Framework Programme for Research of the European Commission, under FET-Open Grant No. 618083 (CN-TQC).

---

\* e-mail: [K.S.Das@rug.nl](mailto:K.S.Das@rug.nl)

† e-mail: [ivan.veramarun@manchester.ac.uk](mailto:ivan.veramarun@manchester.ac.uk)

- [1] M. Johnson and R. H. Silsbee, *Phys. Rev. Lett.* **55**, 1790 (1985).
- [2] F. J. Jedema, A. T. Filip, and B. J. van Wees, *Nature* **410**, 345 (2001).
- [3] F. J. Jedema, H. B. Heersche, A. T. Filip, J. J. A. Baselmans, and B. J. van Wees, *Nature* **416**, 713 (2002).
- [4] F. J. Jedema, M. S. Nijboer, A. T. Filip, and B. J. van Wees, *Phys. Rev. B* **67**, 085319 (2003).
- [5] S. O. Valenzuela and M. Tinkham, *Appl. Phys. Lett.* **85**, 5914 (2004).
- [6] T. Kimura and Y. Otani, *Phys. Rev. Lett.* **99**, 196604 (2007).
- [7] N. Tombros, C. Jozsa, M. Popinciuc, H. T. Jonkman, and B. J. van Wees, *Nature* **448**, 571 (2007).
- [8] T. Kimura, T. Sato, and Y. Otani, *Phys. Rev. Lett.* **100**, 066602 (2008).
- [9] N. Tombros, S. Tanabe, A. Veligura, C. Jozsa, M. Popinciuc, H. T. Jonkman, and B. J. van Wees, *Phys. Rev. Lett.* **101**, 046601 (2008).
- [10] M. H. D. Guimarães, P. J. Zomer, J. Ingla-Aynés, J. C. Brant, N. Tombros, and B. J. van Wees, *Phys. Rev. Lett.* **113**, 086602 (2014).
- [11] I. Žutić, J. Fabian, and S. Das Sarma, *Rev. Mod. Phys.* **76**, 323 (2004).
- [12] H. Idzuchi, Y. Fukuma, S. Takahashi, S. Maekawa, and Y. Otani, *Phys. Rev. B* **89**, 081308 (R) (2014).
- [13] E. Villamor, L. E. Hueso, and F. Casanova, *J. Appl. Phys.* **117**, 223911 (2015).
- [14] F. L. Bakker, A. Slachter, J.-P. Adam, and B. J. van Wees, *Phys. Rev. Lett.* **105**, 136601 (2010).
- [15] See Supplementary Material at <http://> for details on device fabrication, AMR measurements of Py, Hanle fitting, the analytical heat diffusion model, the 3-dimensional finite element modelling (3D-FEM) and checks for inverted Hanle, higher harmonics detection and injection current dependence.
- [16] S. Takahashi and S. Maekawa, *Phys. Rev. B* **67**, 052409 (2003).
- [17] T. Valet and A. Fert, *Phys. Rev. B* **48**, 7099 (1993).
- [18] G. Schmidt, D. Ferrand, L. W. Molenkamp, A. T. Filip, and B. J. van Wees, *Phys. Rev. B* **62**, 4790 (R) (2000).
- [19] G. Mihajlović, J. E. Pearson, S. D. Bader, and A. Hoffmann, *Phys. Rev. Lett.* **104**, 237202 (2010).
- [20] T. G. S. M. Rijks, R. Coehoorn, M. J. M. de Jong, and W. J. M. de Jonge, *Phys. Rev. B* **51**, 283 (1995).
- [21] Y. Fukuma, L. Wang, H. Idzuchi, S. Takahashi, S. Maekawa, and Y. Otani, *Nature Mater.* **10**, 527 (2011).
- [22] S. P. Dash, S. Sharma, J. C. Le Breton, J. Peiro, H. Jaffrés, J.-M. George, A. Lemaître, and R. Jansen, *Phys. Rev. B* **84**, 054410 (2011).
- [23] G. Mihajlović, S. I. Erlingsson, K. Výborný, J. E. Pearson, S. D. Bader, and A. Hoffmann, *Phys. Rev. B* **84**, 132407 (2011).
- [24] J.-E. Wegrowe, Q. A. Nguyen, M. Al-Bark, J.-F. Dayen, T. L. Wade, and H.-J. Drouhin, *Phys. Rev. B* **73**, 134422 (2006).
- [25] A. Slachter, F. L. Bakker, and B. J. van Wees, *Phys. Rev. B* **84**, 020412 (R) (2011).
- [26] R. Mitdank, M. Handweg, C. Steinweg, W. Töllner, M. Daub, K. Nielsch, and S. F. Fischer, *J. Appl. Phys.* **111**, 104320 (2012).
- [27] J. Kimling, J. Gooth, and K. Nielsch, *Phys. Rev. B* **87**, 094409 (2013).
- [28] T. Maassen, I. J. Vera-Marun, M. H. D. Guimarães, and B. J. van Wees, *Phys. Rev. B* **86**, 235408 (2012).
- [29] I. J. Vera-Marun, J. J. van den Berg, F. K. Dejene, and B. J. van Wees, *Nature Commun.* **7**, 11525 (2016).
- [30] M.-H. Bae, Z.-Y. Ong, D. Estrada, and E. Pop, *Nano Lett.* **10**, 4787 (2010).
- [31] S. Hu and T. Kimura, *Phys. Rev. B* **87**, 014424 (2013).